

Tailoring interface epitaxy and magnetism in $\text{La}_{1-x}\text{Sr}_x\text{MnO}_3/\text{SrTiO}_3$ heterostructures via temperature-driven defect engineering

Cite as: J. Appl. Phys. **132**, 105304 (2022); <https://doi.org/10.1063/5.0095406>

Submitted: 05 July 2022 • Accepted: 11 August 2022 • Published Online: 13 September 2022

 Alan Molinari,  Saleh Gorji,  Jan Michalička, et al.



ARTICLES YOU MAY BE INTERESTED IN

[Interface effect of Fe and \$\text{Fe}_2\text{O}_3\$ on the distributions of ion induced defects](#)

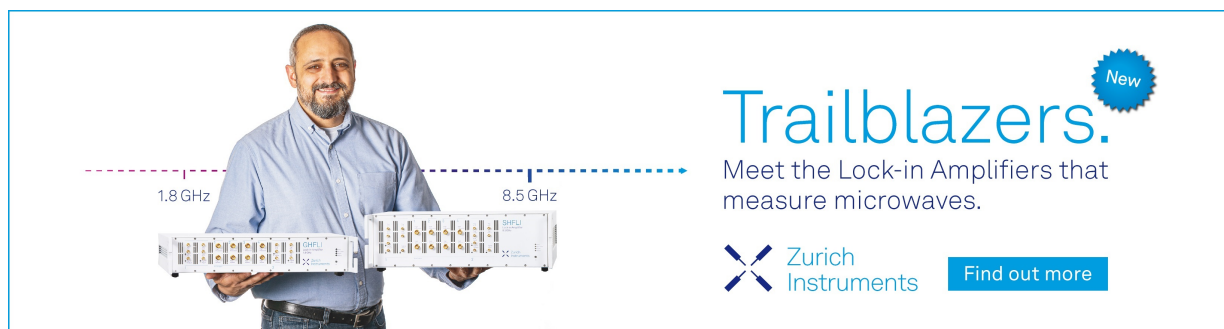
Journal of Applied Physics **132**, 105901 (2022); <https://doi.org/10.1063/5.0095013>

[Electronic structure, magnetic, transport, and optical properties of bulk and film \$\text{Fe}_2\text{CrGa}\$ Heusler alloy. Effect of structural disorder](#)

Journal of Applied Physics **132**, 105103 (2022); <https://doi.org/10.1063/5.0105273>

[Image-based machine learning for materials science](#)

Journal of Applied Physics **132**, 100701 (2022); <https://doi.org/10.1063/5.0087381>



Trailblazers. 

Meet the Lock-in Amplifiers that measure microwaves.

 Zurich Instruments [Find out more](#)

Tailoring interface epitaxy and magnetism in $\text{La}_{1-x}\text{Sr}_x\text{MnO}_3/\text{SrTiO}_3$ heterostructures via temperature-driven defect engineering

Cite as: J. Appl. Phys. **132**, 105304 (2022); doi: 10.1063/5.0095406

Submitted: 5 July 2022 · Accepted: 11 August 2022 ·

Published Online: 13 September 2022



Alan Molinari,^{1,2,a)}  Saleh Gorji,^{2,3}  Jan Michalička,⁴  Christian Kübel,^{2,3,5}  Horst Hahn,^{2,3} 
and Robert Kruk^{2,a)} 

AFFILIATIONS

¹IBM Research Europe—Zurich, Säumerstrasse 4, 8803 Rüschlikon, Switzerland

²Institute of Nanotechnology, Karlsruhe Institute of Technology, Hermann-von-Helmholtz-Platz 1, 76344 Eggenstein-Leopoldshafen, Germany

³KIT-TUD-Joint Research Laboratory Nanomaterials, Technical University Darmstadt, Otto-Berndt-Str. 3, 64287 Darmstadt, Germany

⁴CEITEC Nano Research Infrastructure, Brno University of Technology, Purkyňova 123, 612 00 Brno, Czech Republic

⁵Karlsruhe Nano Micro Facility, Karlsruhe Institute of Technology, Hermann-von-Helmholtz-Platz 1, 76344 Eggenstein-Leopoldshafen, Germany

^{a)}Authors to whom correspondence should be addressed: molinarialan86@gmail.com and robert.kruk@kit.edu

ABSTRACT

Defect engineering of $\text{La}_{1-x}\text{Sr}_x\text{MnO}_3$ (LSMO)—a strongly correlated oxide displaying half metallicity and ferromagnetism above room temperature—has been the focus of a long-standing quest aimed at the exploitation of this material as a functional building block for memory storage and spintronic applications. Here, we discuss the correlation between structural defects and magnetism in $\text{La}_{0.74}\text{Sr}_{0.26}\text{MnO}_3/\text{SrTiO}_3$ (LSMO/STO) epitaxial heterostructures as a function of growth temperature and post-deposition annealing. Upon increasing the growth temperature from 500 to 700 °C at a fixed oxygen partial pressure of 0.007 mbar, the sputter-deposited epitaxial LSMO films experience a progressive increase in Curie temperature T_c from 110 to 270 K and saturation magnetization M_s from 1.4 to 3.3 $\mu_B/\text{u.c.}$ owing to a reduction in oxygen deficiencies. Concurrently, however, growth temperatures above 600 °C trigger the formation of off-stoichiometric, dendritic-like SrMoO_x islands at the film/substrate interface as a possible aftermath of temperature-driven diffusion of impurities from the STO substrate. Notably, although the interfacial spurious islands cause an increase in sample surface roughness, the heterostructure still preserves high-quality epitaxy. In general, the best compromise in terms of both structural and magnetic properties, comprising high-quality epitaxy, atomically flat surface, and robust ferromagnetism above room temperature, is obtained for LSMO films grown at a relatively low temperature of about 500–540 °C followed by a post-deposition annealing treatment at 900 °C for 1 h in air. Our study compares effective routes based on temperature-controlled defect engineering to finely tailor the complex interplay between microstructure and magnetism in LSMO thin films.

© 2022 Author(s). All article content, except where otherwise noted, is licensed under a Creative Commons Attribution (CC BY) license (<http://creativecommons.org/licenses/by/4.0/>). <https://doi.org/10.1063/5.0095406>

INTRODUCTION

$\text{La}_{1-x}\text{Sr}_x\text{MnO}_3$ (LSMO) is a mixed-valence manganese oxide exhibiting an inherent coupling between lattice, charge, and spin degrees of freedom.^{1–6} Such intrinsic correlations lie at the origin of an intriguing interplay between structural, magnetic, and electric properties, including colossal magnetoresistance, half metallicity, metal-to-insulator, and para-to-ferromagnetic transitions in

proximity to room temperature.^{7–16} This unique set of physical properties has denoted LSMO as one of the most attractive constitutive elements to realize spin valves,^{18–20} magnetic field sensors,²¹ magnetoelectric,^{17,22–27} and memristive memories.^{28–31}

The magnetic exchange interactions in LSMO, based on the competition between double- and superexchange mechanisms, can be substantially affected by the presence of structural defects since

they are responsible for altering the bond angle and length along Mn–O–Mn chains and the oxidation state of the Mn ions (i.e., either 3^+ or 4^+).^{8,9,15,16,32–34} For instance, considering the local microstructure of the LSMO lattice, the aftermath of a single oxygen vacancy is (i) to disrupt an exchange interaction and, thus, also the hopping of charge carriers along a Mn–O–Mn chain; (ii) to modify the local oxidation state of Mn ions due to doping with two electrons; and (iii) to distort the bond lengths and angles of the oxygen octahedron surrounding a Mn ion, thus modifying the respective crystal field.^{1,34} Structural defects in LSMO are also considered as one of the principal causes for the occurrence of the so-called magnetic dead layer (MDL),^{33,35–37} which is commonly invoked to explain the lower values of Curie temperature and magnetic moment attained in thin and ultrathin films as compared to bulk LSMO.

From another perspective, structural defects are also of great importance when the purpose is to employ LSMO as a magnetic and/or conducting seed layer in combination with other functional materials, such as dielectrics or ferroelectrics.^{26,30,38,39} Typically, complex epitaxial heterostructures require highest-quality epitaxy since the presence of large interface roughness or surface islands can be responsible for several negative side effects, including reduced interfacial coupling, leakage current, or inefficient spin/charge injection.^{38,40,41}

For these reasons, defect engineering based on the judicious control of the fabrication conditions represents a pivotal aspect for mitigating the detrimental effects of defects on the structural and magnetic properties of LSMO thin films. A common approach is to study the influence of various oxygen pressures during film growth, particularly with the aim of optimizing the oxygen stoichiometry.^{8,9,15,16,42} Often an oxygen pressure of up to 0.1–0.3 mbar is necessary in order to attain properly oxidized LSMO films with robust ferromagnetism; nonetheless, an optimum value of background oxygen pressure is required in order to avoid the emergence of an increased surface roughness due to island formation.^{15,16} Another crucial parameter is represented by the growth temperature T_{gr} , which regulates several aspects of defect engineering, including the film oxidation rate, the migration and nucleation of elemental species on the sample surface, and the film/substrate elemental interdiffusion.^{43,44} Moreover, following film growth, post-deposition annealing under conditions of high temperature and oxygen pressure is an additional tool, which allows to optimize the oxygen stoichiometry and to promote surface reconstruction.¹¹

In this work, we examine the impact of T_{gr} (500–700 °C range) and post-deposition annealing on the correlation between structural defects, particularly oxygen vacancies and impurity islands, and magnetism in epitaxial LSMO films. It is found that a high $T_{\text{gr}} \approx 700$ °C promotes film oxidation and, thus, also better magnetic properties as compared to the films grown at a low $T_{\text{gr}} \approx 500$ °C. However, this occurs at the expense of an increased surface roughness because of the formation of spurious, yet epitaxial islands at the LSMO/STO interface, possibly due to the diffusion of impurities from the bulk of the substrate. As a strategy to mitigate the increased surface roughness, we show that post-deposition annealing of LSMO films grown at low values of $T_{\text{gr}} \approx 500$ –550 °C allows us to concurrently obtain an atomically flat surface and robust ferromagnetism above room temperature.

METHODS

LSMO thin films with a thickness of about 15 nm and a composition of Sr=0.26 were epitaxially grown onto epi-polished, (001)-oriented STO substrates by rf-magnetron sputtering. The pressure during LSMO growth was set to 0.018 mbar in a 3/2 mixture of Ar/O₂, which corresponds to an oxygen partial pressure of 0.007 mbar. The growth temperature T_{gr} , calibrated with a type-K thermocouple (see the [supplementary material](#)), was systematically varied between 500 and 700 °C. After the growth process, the LSMO/STO samples were cooled down to room temperature at a rate of 10 K/min in 0.08 mbar of pure oxygen atmosphere. Microstructure and magnetism of the LSMO samples were investigated before and after carrying out post-deposition annealing treatment at 900 °C for 1 h in air using various experimental methods, including high-resolution x-ray diffraction (HRXRD), atomic force microscopy (AFM), scanning transmission electron microscopy (STEM), and superconducting quantum interference device (SQUID) magnetometry. Further details about experimental methods can be found elsewhere.^{8,45}

RESULTS AND DISCUSSION

Structural analysis by HRXRD reveals that all LSMO films deposited in the 500–700 °C range grow epitaxially following the <001>-orientation of the STO substrate (see [Fig. 1](#)). The presence of pronounced Laue oscillations in proximity of the (002) LSMO reflection indicates the coherent stacking of the LSMO unit cells along the out-of-plane direction, thus confirming a high degree of epitaxial order. The main influence of varying T_{gr} is to induce a systematic shift of the HRXRD peaks of LSMO. For $T_{\text{gr}} \approx 500$ –550 °C, the LSMO and STO peaks almost overlap, whereas upon increasing T_{gr} up to 700 °C, the LSMO reflections systematically shift toward higher angles (see [Fig. 1](#), top), corresponding to a decrease in the out-of-plane lattice parameter of LSMO from about 3.90 to 3.86 Å. It is established that the LSMO unit cell undergoes an expansion along the c-axis in the presence of oxygen deficiencies.^{8,46} Therefore, the progressive shrinkage of the LSMO unit cell at higher values of T_{gr} provides a clear indication of the improvement of the oxygen stoichiometry in the LSMO films. This observation is confirmed by the results of the magnetic characterization described in the following.

The abundant presence of oxygen deficient sites at low T_{gr} is further corroborated by analyzing the effect of post-deposition annealing at 900 °C for 1 h in air on the as-grown LSMO samples. In this case, the HRXRD peaks of all LSMO films, which still feature neat Laue fringes, shift toward a common 2θ value, corresponding to an out-of-plane lattice parameter of about 3.86 Å (see [Fig. 1](#), bottom). This outcome demonstrates that post-deposition annealing treatment permits to adjust the oxygen stoichiometry of all LSMO films in a comparable manner regardless of the initial T_{gr} . Additional XRD analysis, including rocking curves, in-plane LSMO/STO epitaxial relation, and four-fold symmetry are in [Fig. S1](#) in the [supplementary material](#).

The surface morphology of the post-annealed LSMO films grown at various T_{gr} was investigated by AFM (see [Fig. 2](#)). For values of $T_{\text{gr}} < 600$ °C, the LSMO surface is characterized by atomically flat terraces with a height of one or half unit cell steps over

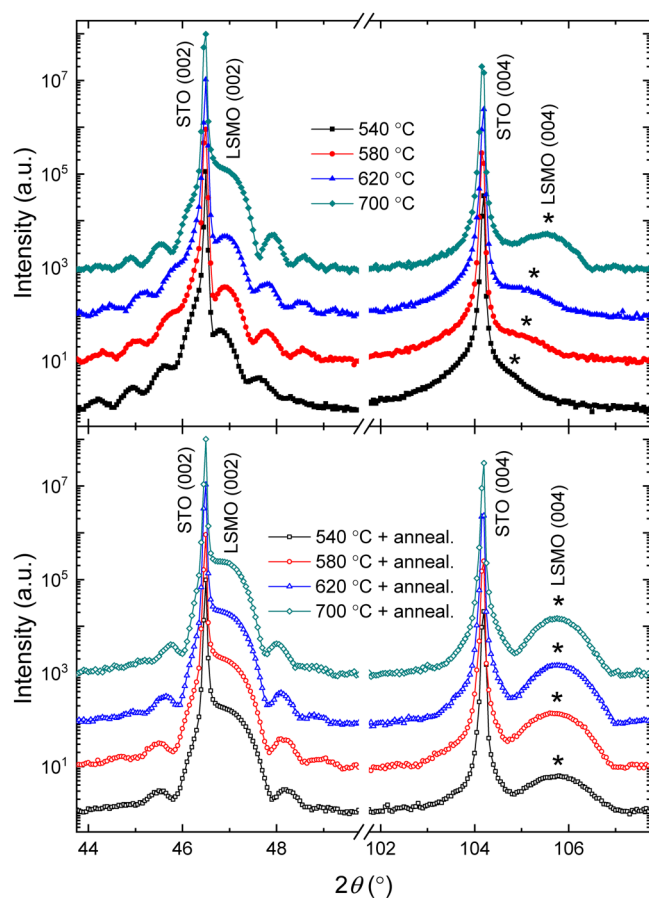


FIG. 1. HRXRD scans of LSMO films with a thickness of 15 nm deposited onto (001)-oriented STO substrate at various growth temperatures (top) and after post-deposition annealing (bottom). Characteristic Laue fringes are visible in proximity of the LSMO (002) reflections. The systematic shift of the LSMO reflections toward higher angles, as indicated by the asterisk symbol, is attributed to a reduction in the amount of oxygen deficiencies.

large areas of several μm^2 and a root mean square (RMS) roughness lower than 0.2 nm. The presence of flat terraces is the result of surface reconstruction after post-deposition annealing since the as-grown films are atomically smooth, but do not have step-like features (see Fig. S2 in the [supplementary material](#)). Above a critical temperature of $T_{\text{gr}} \approx 600^\circ\text{C}$, islands are formed on the LSMO surface, which cause an increased surface roughness, though large portions of the LSMO surface are still covered by flat terraces. An increased surface roughness upon increasing T_{gr} has also been observed in pulsed laser deposited LSMO films.⁴⁷ It is worth to note that at $T_{\text{gr}} \approx 650^\circ\text{C}$, the islands have an average diameter of about 100–200 nm and are randomly distributed on the LSMO surface. Differently, at $T_{\text{gr}} \approx 700^\circ\text{C}$, the LSMO surface presents large dendritic-like islands with a lateral size of about $1\ \mu\text{m}$ separated by wide portions of the LSMO surface with atomically smooth, step-like terraces. This behavior suggests that T_{gr} acts as a driving force

to promote initially island formation (for $T_{\text{gr}} > 600^\circ\text{C}$) and then island coalescence (for $T_{\text{gr}} > 650^\circ\text{C}$).

Previous studies reported on the formation of chemically spurious islands on the top surface of LSMO films due to adatom inhomogeneities that do not overcome a critical island size⁴¹ or strontium segregation driven by a buildup of oxygen vacancy–strontium interactions near the LSMO surface regions.⁴⁸ However, a local inspection of the structural and chemical features of a cross section with an island formed at $T_{\text{gr}} \approx 700^\circ\text{C}$ unveils a different scenario for the process of island formation in our LSMO/STO heterostructures [see STEM and energy dispersive x-ray (EDX) analyses in Fig. 3].

On the one hand, the region of the heterostructure far from the surface island presents a smooth top surface and cube-on-cube arrangement of the LSMO unit cells onto STO [see the right side of Fig. 3(a)], thus corroborating the high crystalline quality and fully strained growth already identified by the HRXRD study. On the other hand, in the proximity of the surface island, it is evident the presence of a crystalline grain formed near the film/substrate interface rather than on top of the LSMO film [see the left side of Fig. 3(a)]. A closer inspection of the film/substrate interface reveals that the spurious grain is not directly in contact with the STO substrate but lies onto a few unit cells of LSMO. Most strikingly, despite the interfacial grain, the heterostructure maintains a coherent epitaxial growth with the underlying STO substrate, including the LSMO film on top, as also evidenced by the Fast Fourier Transform analysis in Fig. 3(b). Concerning the chemical composition, EDX analysis [Fig. 3(c)] reveals that the interfacial grain is composed of a SrMoO_x phase, whereas the other regions of the heterostructure correspond to LSMO and STO.

The source of the Mo contamination is unclear; here, we provide some possible interpretations. It is unlikely that the origin of the interfacial SrMoO_x islands is related to volatile Mo species being transferred in the vapor phase from nearby contaminated heat sources (e.g., substrate susceptor, clamp, heater block, etc.) onto the LSMO/STO samples during film growth. Indeed, in such circumstances, one would expect the Mo species to be progressively and uniformly embedded in the LSMO film during the growth process and, thus, to nucleate into Mo-rich grains spread at various depth of the LSMO thickness (or possibly at the LSMO surface in order to minimize surface energies). Such a spread distribution of SrMoO_x grains does not occur in our LSMO/STO heterostructures. As corroborated by the STEM–EDX analysis in Figs. S4–S8 in the [supplementary material](#), the Mo-rich spurious grains are always located at the LSMO/STO interface.

Furthermore, we carried out an additional control experiment to stress the fact that Mo impurities are not caused by crosstalk contamination from other sputtering targets (which anyway do not contain Mo) and that T_{gr} is the driving force for the formation of such grains at the LSMO/STO interface. Indeed, after simply exposing an original STO substrate to a temperature of 700°C inside the sputtering chamber (without LSMO deposition), dendritic-like islands form on its surface (see Fig. S3 in the [supplementary material](#)).

As a final remark, we note that, according to the EDX analysis in Fig. 3(c), the grains are uniformly composed not only of elemental Mo but also Sr. The fact that both Sr and Mo species are present within the spurious grains at the film/substrate interface hints at a common origin for such elements.

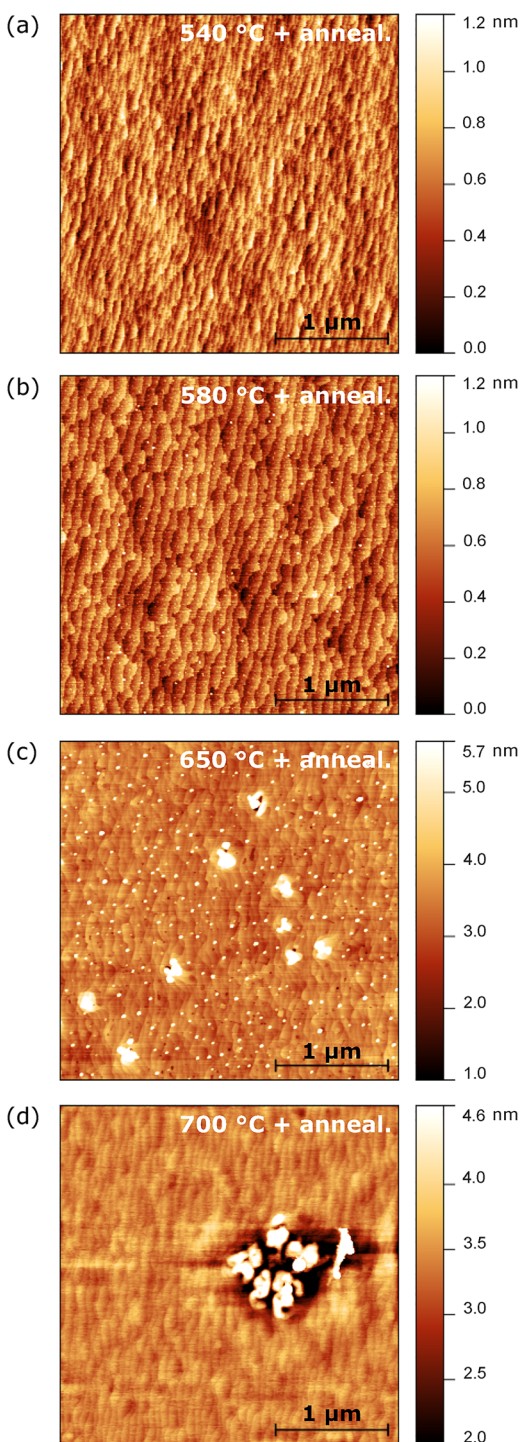


FIG. 2. (a)–(d) AFM images of the LSMO films grown at various temperatures after carrying out post-deposition annealing treatment. The surface morphology presents atomically flat terraces over large areas, but islands are formed on the LSMO surface at temperatures beyond 600 °C [(c) and (d)].

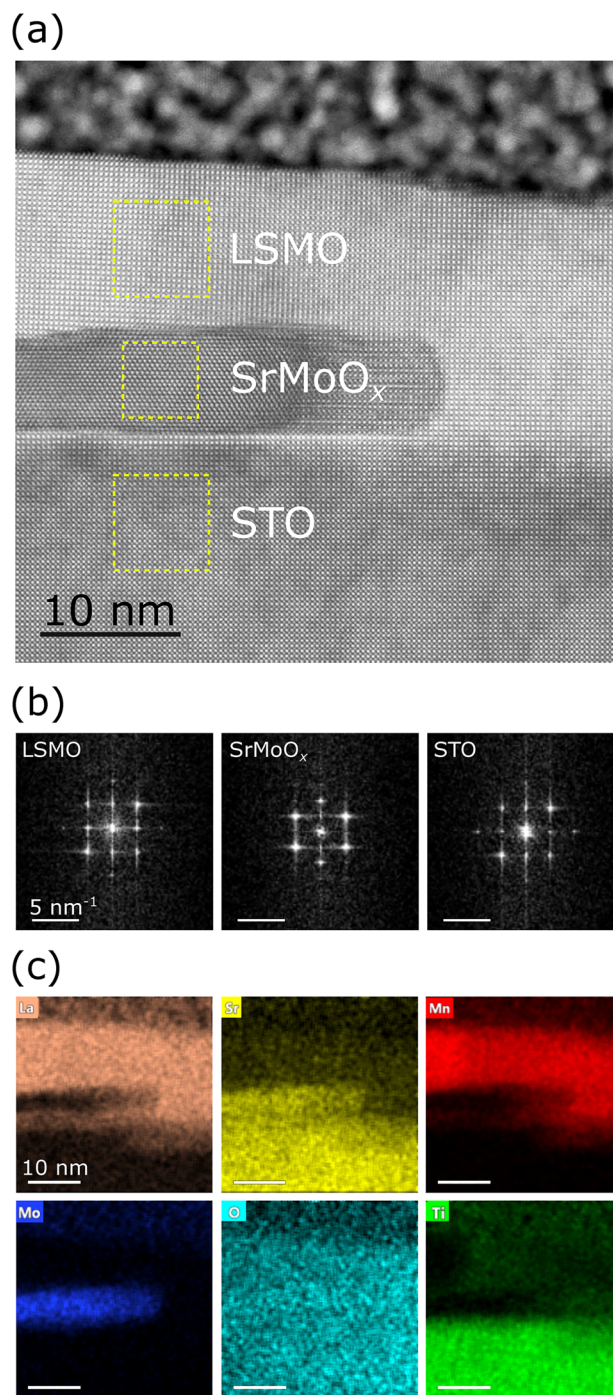


FIG. 3. (a) STEM analysis of a representative LSMO/STO cross section for a sample grown at 700 °C. A spurious SrMoO_x grain is located at the LSMO/STO interface. Despite the interfacial grain, LSMO film epitaxy with cube-on-cube arrangement of the LSMO unit cells is preserved in the whole investigated area. (b) FFT patterns of the LSMO film on top of the interfacial grain, the SrMoO_x grain, and the STO substrate. (c) EDX analysis of the STEM cross section.

In the light of these observations and the experimental results of AFM, STEM, and EDX surveys, we attribute the presence of SrMoO_x grains at the film/substrate interface to temperature-driven diffusion of Sr and Mo species intrinsic in the bulk of the STO substrates. We note that, although previous works on LSMO/STO heterostructures did not report on the formation of spurious interfacial SrMoO_x grains and that Mo is not a conventional impurity in STO substrate, the role of defect chemistry and the importance of background impurities in undoped STO are still under intensive evaluation.^{49–51}

In a plausible scenario, during the initial stages of film growth at $T_{gr} > 600$ °C, the interfacial islands are small enough to permit the formation of a few coherent and continuous layers of LSMO onto the STO substrate. As the deposition advances, more and more impurities diffuse from the STO substrate and provoke the expansion of the interfacial grains, which are progressively covered by the growing LSMO film. Concerning the evolution of the interfacial spurious grains as a function of T_{gr} (see Fig. 4), we note from the AFM analysis in Fig. 2 that below 600 °C, the LSMO surface appears atomically flat. Above 600 °C, small islands with no preferential spatial distribution start to be visible on the LSMO surface, whereas larger agglomerates are formed upon increasing T_{gr} up to 700 °C. This observation suggests that the use of a higher T_{gr} enhances the diffusion of Sr and Mo species toward the LSMO/STO interface. Then, high mobile Sr and Mo interfacial species lead to the nucleation and coalescence of extensive SrMoO_x grains. The simplified scenario proposed in Fig. 4 resembles some of the features observed in the case of the anomalous diffusion at metal/ceramic interfaces.⁵²

Previous works already reported on the creation of Sr-rich surface islands in the case of doped and stoichiometric STO single crystals at temperatures of 1000–1100 °C under ambient pressure.^{53–55} In our case, we ascribe the formation of surface islands onto the STO substrate already at temperatures as low as 650 °C to a combination of thermal stress, substrate clamping, and reducing atmosphere, which facilitate the formation of dislocations in STO and the subsequent diffusion of bulk impurities toward its surface. Furthermore, nanometer-size voids identified at the surface

of both original and chemically treated STO substrates by means of AFM analysis are suspected to act as preferential paths for the diffusion of impurities from inner regions of STO (see Fig. S10 in the supplementary material).

As a possible alternative scenario, we cannot completely rule out the eventuality that Mo impurities are inherent in the bulk of the stainless-steel holder clamping the STO substrate rather than in the STO substrate itself. We also stress that a specific sample holder dedicated for the growth of LSMO films was employed and such holder has never been previously exposed to Mo deposition. In this case, it is plausible that a high temperature may trigger the diffusion of intrinsic Mo species from the stainless-steel holder to the STO substrate and eventually to the LSMO/STO interface. Even in the circumstances that the STO substrate acts as medium rather than a reservoir of Mo impurities, the general mechanisms of diffusion and nucleation of interfacial SrMoO_x grains proposed in Fig. 4 still hold.

The influence of T_{gr} and post-deposition annealing on the magnetic properties of epitaxial LSMO thin films with a thickness of about 15 nm is shown in Fig. 5. The magnetic field-cooled $M(T)$ curves of the as-grown LSMO films display a progressive increase in Curie temperature T_c from 110 to 270 K upon increasing T_{gr} from 500 to 700 °C [Fig. 5(a), top]; the derivatives of the $M(T)$ curves present a FWHM of about 48 K, thus indicating a rather smeared out para–ferromagnetic transition [Fig. 5(a), bottom]. Concurrently, the saturation magnetization M_s measured at 10 K reveals a systematic increase from 1.4 to 3.3 μ_B /u.c. [Fig. 5(b)]. The improvement in T_c and M_s at higher values of T_{gr} supports the idea of a strong reduction in the amount of oxygen vacancies in LSMO, thus corroborating the results of the XRD analysis discussed above.

After carrying out post-deposition annealing on the as-grown LSMO films, all samples exhibit similar magnetic characteristics with an increased $T_c \approx 320$ K, a sharper magnetic transition (FWHM of $dM/dT \approx 25$ K) and M_s above 3 μ_B /u.c. In particular, after post-deposition annealing, the LSMO film grown at the lowest temperature of 500 °C undergoes a massive jump in T_c of about 200 K and the value of M_s more than doubles. The results of

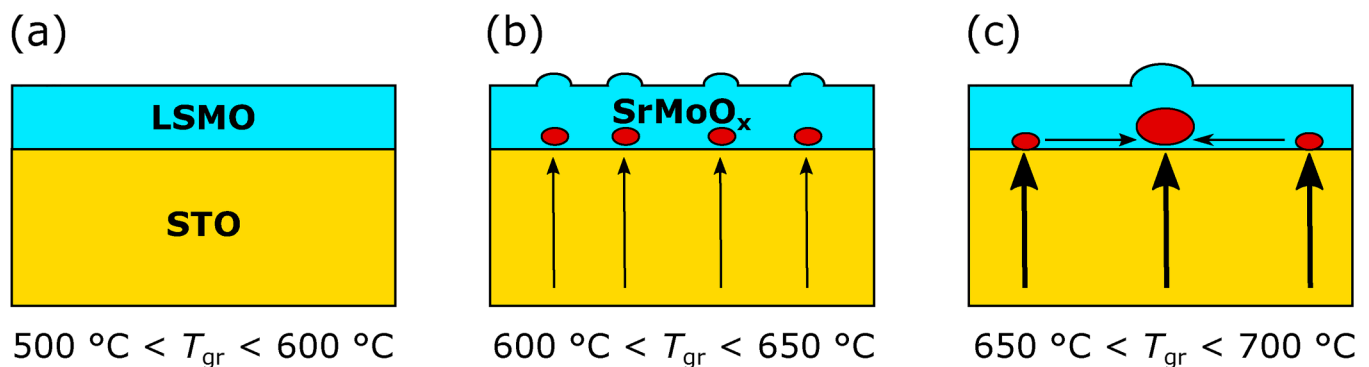


FIG. 4. Sketch of the growth processes occurring in LSMO/STO heterostructures at different growth temperatures. (a) LSMO films grown at $T_{gr} < 600$ °C are atomically flat. (b) Above $T_{gr} > 600$ °C, sub-micrometer SrMoO_x islands are formed at the LSMO/STO interface due to the diffusion of Sr and Mo impurities from bulk STO. (c) At $T_{gr} \approx 700$ °C, larger micrometer-sized interfacial islands are created due to the enhanced mobility and coalescence of Sr and Mo species.

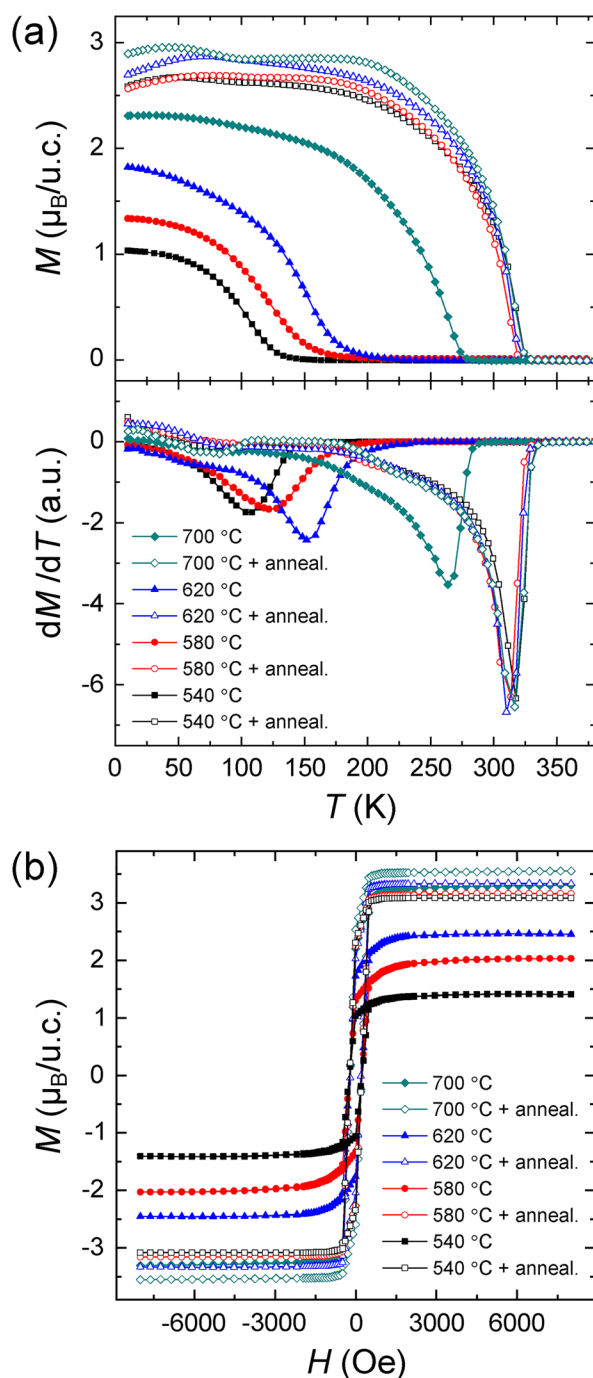


FIG. 5. (a) Magnetization and derivative curves as a function of temperature for LSMO films grown at different temperatures (filled symbols) and after post-deposition annealing (empty symbols). A magnetic field of 100 Oe was applied parallel to the in-plane film direction. (b) Magnetic hysteresis loops carried out at 10 K. The systematic increase in magnetic moment and Curie temperature upon increasing the growth temperature or after carrying out post-deposition annealing is attributed to an improvement of the LSMO oxygen stoichiometry.

structural and magnetic characterization suggest that the post-annealed LSMO films grown at a relatively low $T_{\text{gr}} \approx 500\text{--}540\text{ }^\circ\text{C}$ are the best candidates for implementation in complex multilayer heterostructures since they combine an ideal surface smoothness and robust ferromagnetism above room temperature. Further insights into the possible role of a magnetic dead layer in such optimized LSMO films are discussed in the [supplementary material](#).

We also note that, although all samples were exposed to the same post-deposition annealing protocol, the LSMO film grown at 700 °C reaches the highest M_s of about $3.5\ \mu_B/\text{u.c.}$ On the one hand, this is possibly related to a more uniform and complete oxidation achieved throughout the whole LSMO film thickness during the growth process; on the other hand, the use of a high T_{gr} of 700 °C may favor the formation of straightest Mn–O–Mn bonds, as supported by the sharpest rocking curves obtained in the XRD analysis (see Fig. S1 in the [supplementary material](#)). Besides, if we consider a hypothetical scenario where Sr species shall primarily diffuse from the LSMO film—rather than the STO substrate—to form the interfacial SrMoO_x spurious grains, then one would expect a decrease in T_c and M_s , because for the composition of our $\text{La}_{1-x}\text{Sr}_x\text{MnO}_3$ films ($x \approx 0.26$), a reduction in Sr content is expected to weaken double-exchange interactions (see LSMO phase diagram in Refs. 4 and 6). On the contrary, the LSMO film grown at 700 °C, that is the one with biggest interfacial SrMoO_x islands, presents the highest values of T_c and M_s . Therefore, the results of the magnetic characterization offer another clue for the temperature-driven diffusion of impurities from the bulk STO substrate. Moreover, it can also be concluded that the SrMoO_x islands formed at the film/substrate interface do not dramatically affect magnetism in the LSMO films, if not possibly on a local scale.

CONCLUSIONS

In this work, the structural and magnetic properties of epitaxial LSMO/STO heterostructures were examined in the framework of defect engineering upon control of T_{gr} (500–700 °C) and post-deposition annealing conditions. On the one hand, oxygen vacancies, whose concentration diminishes when increasing T_{gr} or after carrying out post-deposition annealing, are the main contributors defining the robustness of ferromagnetism in LSMO thin films. On the other hand, for $T_{\text{gr}} > 600\text{ }^\circ\text{C}$, spurious SrMoO_x grains are formed at the LSMO/STO interface, which in turn induce an increase in LSMO surface roughness. The process of formation of interfacial SrMoO_x defects, possibly ascribed to the diffusion of Sr and Mo impurities inherent in the STO substrate due to the combined effects of thermal stress, reducing atmosphere, substrate clamping, and nanometer-size voids at the STO surface, deserves more in-depth analysis and modeling in future studies. Furthermore, insights about the influence of the interfacial SrMoO_x grains on the local magnetism of LSMO may be obtained by carrying out Lorentz-TEM analysis. Combining the results of our experimental survey, state-of-the-art LSMO films with best compromise in terms of crystalline quality, surface smoothness, and ferromagnetic properties are attained when employing a relatively low $T_{\text{gr}} \approx 500\text{--}540\text{ }^\circ\text{C}$ followed by post-deposition annealing. To conclude, our study evaluates functional strategies to engineer temperature-driven defects in epitaxial LSMO thin films, hence promoting the

exploitation of LSMO in complex multilayer heterostructures for potential spintronic applications.

SUPPLEMENTARY MATERIAL

See the [supplementary material](#) for more details on the structural and magnetic characterization related to the present study.

ACKNOWLEDGMENTS

The authors acknowledge Philipp Leufke and Ralf Witte for support in the fabrication and characterization of LSMO films. This project has received funding from the European Union's Horizon 2020 Research and Innovation Program under Marie Skłodowska-Curie Grant Agreement No. 898113 (InNaTo), from the Deutsche Forschungsgemeinschaft (DFG) under Project Nos. LE 3519/1-2 and MU 333/2-2, and as part of the DFG Research Group 2093 (memristive elements for neural systems) under Project No. CH 1492/1-1. Saleh Gorji acknowledges his Ph.D. scholarship by the DAAD. The authors acknowledge the support of the Karlsruhe Nano Micro Facility (KNMF) for the use of various experimental facilities and CzechNanoLab Research Infrastructure supported by MEYS CR (No. LM2018110) for TEM measurements.

AUTHOR DECLARATIONS

Conflict of Interest

The authors have no conflicts to disclose.

Author Contributions

Alan Molinari: Conceptualization (lead); Data curation (equal); Formal analysis (equal); Investigation (equal); Methodology (equal); Validation (equal); Visualization (lead); Writing – original draft (lead); Writing – review & editing (lead). **Saleh Gorji:** Formal analysis (equal); Investigation (equal); Visualization (equal); Writing – review & editing (supporting). **Jan Michalička:** Formal analysis (equal); Investigation (equal); Visualization (equal); Writing – review & editing (supporting). **Christian Kübel:** Formal analysis (equal); Supervision (equal); Writing – review & editing (supporting). **Horst Hahn:** Conceptualization (supporting); Funding acquisition (lead); Resources (lead); Writing – review & editing (supporting). **Robert Kruk:** Conceptualization (supporting); Funding acquisition (equal); Project administration (equal); Resources (equal); Supervision (equal); Writing – review & editing (supporting). **Robert Kruk:** Conceptualization (supporting); Funding acquisition (equal); Project administration (equal); Resources (equal); Supervision (equal); Writing – review & editing (supporting).

DATA AVAILABILITY

The data that support the findings of this study are available from the corresponding authors upon reasonable request.

REFERENCES

- ¹E. Dagotto, T. Hotta, and A. Moreo, *Phys. Rep.* **344**, 1 (2001).
- ²Y. Tokura and Y. Tomioka, *J. Magn. Magn. Mater.* **200**, 1 (1999).

- ³K. Dörr, *J. Phys. D: Appl. Phys.* **39**, R125 (2006).
- ⁴O. Chmaissem, B. Dabrowski, S. Kolesnik, J. Mais, J. D. Jorgensen, and S. Short, *Phys. Rev. B* **67**, 944311 (2003).
- ⁵B. Dabrowski, X. Xiong, Z. Bukowski, R. Dybziński, P. W. Klamut, J. E. Siewenie, O. Chmaissem, J. Shaffer, C. W. Kimball, J. D. Jorgensen, and S. Short, *Phys. Rev. B* **60**, 7006 (1999).
- ⁶J. Hemberger, A. Krimmel, T. Kurz, H. A. Krug von Nidda, V. Y. Ivanov, A. A. Mukhin, A. M. Balbashov, and A. Loidl, *Phys. Rev. B* **66**, 094410 (2002).
- ⁷H. Boschker, M. Huijben, A. Vaillonis, J. Verbeeck, S. van Aert, M. Luysberg, S. Bals, G. van Tendeloo, E. P. Houwman, G. Koster, D. H. A. Blank, and G. Rijnders, *J. Phys. D: Appl. Phys.* **44**, 205001 (2011).
- ⁸P. M. Leufke, A. K. Mishra, A. Beck, D. Wang, C. Kübel, R. Kruk, and H. Hahn, *Thin Solid Films* **520**, 5521 (2012).
- ⁹D. Rasic, R. Sachan, N. K. Temizer, J. Prater, and J. Narayan, *ACS Appl. Mater. Interfaces* **10**, 21001 (2018).
- ¹⁰U. K. Sinha, B. Das, and P. Padhan, *Nanoscale Adv.* **2**, 2792 (2020).
- ¹¹L. Cao, O. Petravic, P. Zakalek, A. Weber, U. Rücker, J. Schubert, A. Koutsoubas, S. Mattauch, and T. Brückel, *Adv. Mater.* **31**, 1806183 (2019).
- ¹²B. Paudel, B. Zhang, Y. Sharma, K. T. Kang, H. Nakotte, H. Wang, and A. Chen, *Appl. Phys. Lett.* **117**, 081903 (2020).
- ¹³S. K. Chaluvadi, F. Ajejas, P. Orgiani, S. Lebargy, A. Minj, S. Flament, J. Camarero, P. Perna, and L. Méchin, *J. Phys. D: Appl. Phys.* **53**, 375005 (2020).
- ¹⁴P. Zhou, Y. Qi, C. Yang, Z. Mei, A. Ye, K. Liang, Z. Ma, Z. Xia, and T. Zhang, *AIP Adv.* **6**, 125044 (2016).
- ¹⁵K. Wang, M. H. Tang, Y. Xiong, G. Li, Y. G. Xiao, W. L. Zhang, Z. P. Wang, Z. Li, and J. He, *RSC Adv.* **7**, 31327 (2017).
- ¹⁶S. Kumari, N. Mottaghi, C.-Y. Huang, R. Trappen, G. Bhandari, S. Yousefi, G. Cabrera, M. S. Seehra, and M. B. Holcomb, *Sci. Rep.* **10**, 3659 (2020).
- ¹⁷A. Molinari, H. Hahn, and R. Kruk, *Adv. Mater.* **30**, 1703908 (2018).
- ¹⁸Y. Ogimoto, M. Izumi, A. Sawa, T. Manako, H. Sato, H. Akoh, M. Kawasaki, and Y. Tokura, *Jpn. J. Appl. Phys.* **42**, L369 (2003).
- ¹⁹Y. Yin, X. Jiang, M. A. Koten, J. E. Shield, X. Chen, Y. Yun, A. T. N'Diaye, X. Hong, and X. Xu, *Phys. Rev. Appl.* **13**, 064011 (2020).
- ²⁰F. Y. Bruno, M. N. Grisolia, C. Visani, S. Valencia, M. Varela, R. Abrudan, J. Tornos, A. Rivera-Calzada, A. A. Únal, S. J. Pennycook, Z. Sefrioui, C. Leon, J. E. Villegas, J. Santamaria, A. Barthélémy, and M. Bibes, *Nat. Commun.* **6**, 6306 (2015).
- ²¹O. Rousseau, S. Flament, B. Guillet, M. L. C. Sing, and L. Méchin, *Proceedings* **1**, 635 (2017).
- ²²D. Pesquera, E. Khestanova, M. Ghidini, S. Zhang, A. P. Rooney, F. Maccherozzi, P. Riego, S. Farokhipoor, J. Kim, X. Moya, M. E. Vickers, N. A. Stelmashenko, S. J. Haigh, S. S. Dhesi, and N. D. Mathur, *Nat. Commun.* **11**, 3190 (2020).
- ²³S. M. Wu, S. A. Cybart, P. Yu, M. D. Rossell, J. X. Zhang, R. Ramesh, and R. C. Dynes, *Nat. Mater.* **9**, 756 (2010).
- ²⁴A. Quindeau, I. Fina, X. Marti, G. Apachitei, P. Ferrer, C. Nicklin, E. Pippel, D. Hesse, and M. Alexe, *Sci. Rep.* **5**, 1 (2015).
- ²⁵A. Molinari, H. Hahn, and R. Kruk, *Adv. Mater.* **31**, 1806662 (2019).
- ²⁶D. Yi, P. Yu, Y. Chen, H. Lee, Q. He, Y. Chu, and R. Ramesh, *Adv. Mater.* **31**, 1806335 (2019).
- ²⁷C. Jin, Y. Zhu, W. Han, Q. Liu, S. Hu, Y. Ji, Z. Xu, S. Hu, M. Ye, and L. Chen, *Appl. Phys. Lett.* **117**, 252902 (2020).
- ²⁸N. Zurauskienė, R. Lukose, S. Balevicius, V. Stankevicius, S. Kersulis, V. Plausinaitienė, M. Vagner, and R. Navickas, *IEEE Magn. Lett.* **10**, 1 (2019).
- ²⁹C. Moreno, C. Munuera, X. Obradors, and C. Ocal, *Beilstein J. Nanotechnol.* **3**, 722 (2012).
- ³⁰A. Molinari, R. Witte, K. K. Neelisetty, S. Gorji, C. Kübel, I. Münch, F. Wöhler, L. Hahn, S. Hengsbach, K. Bade, H. Hahn, and R. Kruk, *Adv. Mater.* **32**, 1907541 (2020).
- ³¹L. Wang, C. Yang, J. Wen, S. Gai, and Y. Peng, *J. Mater. Sci. Mater. Electron.* **26**, 4618 (2015).
- ³²X. Wang, C. Jin, P. Wang, X. Pang, W. Zheng, D. Zheng, Z. Li, R. Zheng, and H. Bai, *Appl. Phys. Lett.* **115**, 182405 (2019).

- ³³R. Herger, P. R. Willmott, C. M. Schlepütz, M. Björck, S. A. Pauli, D. Martocchia, B. D. Patterson, D. Kumah, R. Clarke, Y. Yacoby, and M. Döbeli, *Phys. Rev. B* **77**, 085401 (2008).
- ³⁴J. M. D. Coey, M. Viret, and S. von Molnár, *Adv. Phys.* **58**, 571 (2009).
- ³⁵M. Huijben, L. W. Martin, Y. H. Chu, M. B. Holcomb, P. Yu, G. Rijnders, D. H. A. Blank, and R. Ramesh, *Phys. Rev. B* **78**, 094413 (2008).
- ³⁶P. M. Leufke, R. Kruk, R. A. Brand, and H. Hahn, *Phys. Rev. B* **87**, 094416 (2013).
- ³⁷M. Angeloni, G. Balestrino, N. G. Boggio, P. G. Medaglia, P. Orgiani, and A. Tebano, *J. Appl. Phys.* **96**, 6387 (2004).
- ³⁸P. M. Leufke, R. Kruk, D. Wang, C. Kübel, and H. Hahn, *AIP Adv.* **2**, 032184 (2012).
- ³⁹S. Valencia, A. Crassous, L. Bocher, V. Garcia, X. Moya, R. O. Cherifi, C. Deranlot, K. Bouzehouane, S. Fusil, A. Zobelli, A. Gloter, N. D. Mathur, A. Gaupp, R. Abrudan, F. Radu, A. Barthélémy, and M. Bibes, *Nat. Mater.* **10**, 753 (2011).
- ⁴⁰C. Thiele, K. Dörr, O. Bilani, J. Rödel, and L. Schultz, *Phys. Rev. B* **75**, 054408 (2007).
- ⁴¹A. Gambardella, P. Graziosi, I. Bergenti, M. Prezioso, D. Pullini, S. Milita, F. Biscarini, and V. A. Dediu, *Sci. Rep.* **4**, 5353 (2014).
- ⁴²R. Trappen, A. J. Grutter, C. Y. Huang, A. Penn, N. Mottaghi, S. Yousefi, A. Haertter, S. Kumari, J. Lebeau, B. J. Kirby, and M. B. Holcomb, *J. Appl. Phys.* **126**, 105301 (2019).
- ⁴³L. W. Martin, Y. H. Chu, and R. Ramesh, *Mater. Sci. Eng. R Rep.* **68**, 89 (2010).
- ⁴⁴M. Brahlek, A. Sen Gupta, J. Lapano, J. Roth, H. T. Zhang, L. Zhang, R. Haislmaier, and R. Engel-Herbert, *Adv. Funct. Mater.* **28**, 1702772 (2018).
- ⁴⁵A. Molinari, P. M. Leufke, C. Reitz, S. Dasgupta, R. Witte, R. Kruk, and H. Hahn, *Nat. Commun.* **8**, 15339 (2017).
- ⁴⁶T. Petrisor, M. S. Gabor, A. Boule, C. Bellouard, C. Tiusan, O. Pana, and T. Petrisor, *J. Appl. Phys.* **109**, 123913 (2011).
- ⁴⁷S. Majumdar, H. Huhtinen, H. S. Majumdar, R. Laiho, and R. Österbacka, *J. Appl. Phys.* **104**, 033910 (2008).
- ⁴⁸T. T. Fister, D. D. Fong, J. A. Eastman, P. M. Baldo, M. J. Highland, P. H. Fuoss, K. R. Balasubramaniam, J. C. Meador, and P. A. Salvador, *Appl. Phys. Lett.* **93**, 151904 (2008).
- ⁴⁹P. C. Bowes, J. N. Baker, J. S. Harris, B. D. Behrhorst, and D. L. Irving, *Appl. Phys. Lett.* **112**, 022902 (2018).
- ⁵⁰T. Shi, Y. Chen, and X. Guo, *Prog. Mater. Sci.* **80**, 77 (2016).
- ⁵¹M. Siebenhofer, F. Baiutti, J. de Dios Sirvent, T. M. Huber, A. Viernstein, S. Smetaczek, C. Herzig, M. O. Liedke, M. Butterling, A. Wagner, E. Hirschmann, A. Limbeck, A. Tarancon, J. Fleig, and M. Kubicek, *J. Eur. Ceram. Soc.* **42**, 1510 (2022).
- ⁵²A. Kumar, H. Barda, L. Klinger, M. W. Finnis, V. Lordi, E. Rabkin, and D. J. Srolovitz, *Nat. Commun.* **9**, 5251 (2018).
- ⁵³K. Szot, W. Speier, U. Breuer, R. Meyer, J. Szade, and R. Waser, *Surf. Sci.* **460**, 112 (2000).
- ⁵⁴K. Szot and W. Speier, *Phys. Rev. B* **60**, 5909 (1999).
- ⁵⁵Y. Liang and D. A. Bonnell, *Surf. Sci.* **310**, 128 (1994).